**UNIVERSIDAD SAN FRANCISCO DE QUITO USFQ**

**Colegio de Ciencias e Ingenierías**

# Comparative Experimental Evaluation of PID Controllers for 1-DOF Quanser Aero 2

**William Wladimir Cruz Quimbiulco**

**Ana Emilia Ludeña Rueda**

**Electrónica y Automatización**

Trabajo de fin de carrera presentado como requisito
para la obtención del título de
Ingeniera en Electrónica

Quito, Mayo de 2025

# UNIVERSIDAD SAN FRANCISCO DE QUITO USFQ

**Colegio de Ciencias e Ingenierías**

**HOJA DE CALIFICACIÓN**

**DE TRABAJO DE FIN DE CARRERA**

**Comparative Experimental Evaluation of PID Controllers for 1-DOF Quanser Aero 2.**

**William Wladimir Cruz Quimbiulco**

**Ana Emilia Ludeña Rueda**

Tutor: Óscar Camacho, Ph.D.

Quito, Mayo de 2025

# © DERECHOS DE AUTOR

Por medio del presente documento certifico que he leído todas las Políticas y Manuales de la Universidad San Francisco de Quito USFQ, incluyendo la Política de Propiedad Intelectual USFQ, y estoy de acuerdo con su contenido, por lo que los derechos de propiedad intelectual del presente trabajo quedan sujetos a lo dispuesto en esas Políticas.

Asimismo, autorizo a la USFQ para que realice la digitalización y publicación de este trabajo en el repositorio virtual, de conformidad a lo dispuesto en la Ley Orgánica de Educación Superior del Ecuador.



| | |
|---|---|
| Nombres y apellidos: | William Wladimir Cruz Quimbiulco |
| Código: | 00207454 |
| C.I.: | 1723908933 |
| Fecha: | Quito, Mayo de 2025 |

# © DERECHOS DE AUTOR

Por medio del presente documento certifico que he leído todas las Políticas y Manuales de la Universidad San Francisco de Quito USFQ, incluyendo la Política de Propiedad Intelectual USFQ, y estoy de acuerdo con su contenido, por lo que los derechos de propiedad intelectual del presente trabajo quedan sujetos a lo dispuesto en esas Políticas.

Asimismo, autorizo a la USFQ para que realice la digitalización y publicación de este trabajo en el repositorio virtual, de conformidad a lo dispuesto en la Ley Orgánica de Educación Superior del Ecuador.

Nombres y apellidos: Ana Emilia Ludeña Rueda

Código: 00321134

C.I.: 172491126

Fecha: Quito, Mayo de 2025

# ACLARACIÓN PARA PUBLICACIÓN

**Nota:** El presente trabajo, en su totalidad o cualquiera de sus partes, no debe ser considerado como una publicación, incluso a pesar de estar disponible sin restricciones a través de un repositorio institucional. Esta declaración se alinea con las prácticas y recomendaciones presentadas por el Committee on Publication Ethics COPE descritas por Barbour et al. (2017) Discussion document on best practice for issues around theses publishing, disponible en `http://bit.ly/COPETheses`

# UNPUBLISHED DOCUMENT

**Note:** The following capstone project is available through Universidad San Francisco de Quito USFQ institutional repository. Nonetheless, this project – in whole or in part – should not be considered a publication. This statement follows the recommendations presented by the Committee on Publication Ethics COPE described by Barbour et al. (2017) Discussion document on best practice for issues around theses publishing available on `http://bit.ly/COPETheses`

# RESUMEN

Este trabajo evalúa diversas estrategias de control PID en el sistema Quanser Aero 2 con un grado de libertad (1-DOF). El controlador PID clásico se utiliza como referencia y se compara con estrategias mejoradas como el PID 2-DOF, el PID fraccionario, el PID no lineal (todos basados en modelo) y el controlador iPI (libre de modelo). Estas estrategias se analizan en cuanto a su desempeño ante diferentes cambios de referencia y perturbaciones externas. La elección de la configuración 1-DOF se relaciona con aplicaciones reales, como el control de cabeceo en vehículos aéreos no tripulados (UAV) durante el despegue y el aterrizaje. Para garantizar evaluaciones objetivas y consistentes, los parámetros de los controladores fueron optimizados mediante algoritmos genéticos. Las métricas de desempeño consideradas incluyen el Integral del Error Absoluto (IAE), el Integral del Cuadrado de la Señal de Control (ISCO), el sobreimpulso máximo y el tiempo de establecimiento. Los resultados obtenidos resaltan los beneficios y compromisos de cada estrategia en aplicaciones aeroespaciales.

***Palabras clave*:** Control PID, Quanser Aero 2, 1-DOF, PID clásico, PID 2-DOF, FOPID, NPID, iPI, evaluación de desempeño

# ABSTRACT

This paper evaluates various PID controller strategies on the 1-DOF Quanser Aero 2 system. The classical PID controller serves as a reference, compared to improved strategies like 2-DOF PID, fractional-order PID, nonlinear PID (all model-based), and model-free iPI. These are assessed for performance improvement under different reference signals and disturbances. The choice of 1-DOF configuration relates to real-world applications, such as UAV pitch control during takeoff and landing. Consistent and unbiased evaluations were ensured by optimizing controller parameters using genetic algorithms. Performance metrics include Integral of Absolute Error (IAE), Integral of Squared Control Output (ISCO), maximum overshoot, and settling time. Results highlight the benefits and trade-offs of each strategy in aerospace

***Keywords*:** PID control, Quanser Aero 2, 1-DOF, classical PID, 2-DOF PID, FOPID, NPID, iPI, performance evaluation

# CONTENTS

# List of Figures



# List of Tables

# DEDICATORIA

Dedico este logro a mi madre, Adriana, quien ha sido mi principal apoyo, mi fuerza y mi fuente constante de confianza. Gracias a su paciencia, dedicación y esfuerzo, pude llegar hasta aquí, incluso cuando en ocasiones dudaba de lograrlo. Su amor incondicional me ha acompañado en cada paso de este camino.

*William Cruz*

Dedico este hito en mi vida a mi familia, en especial a mis padres y a mi hermana, por su constante apoyo, por creer en mí y acompañarme en cada etapa, especialmente en los momentos más difíciles. Asimismo, deseo dedicar este trabajo a mí misma, por no rendirme y mantenerme firme ante cada desafío. Esta meta representa un avance significativo en mi desarrollo profesional y personal, fruto de perseverancia, esfuerzo y convicción.

*Ana Emilia Ludeña*

# AGRADECIMIENTO

A mi profesor y tutor de tesis, Óscar Camacho, por su apoyo en los momentos de duda en la carrera, por su paciencia y la confianza que siempre tuvo en mí. Su orientación y constante apoyo fueron clave para superar los desafíos durante este proceso.

A mi tía Carmen, por su cuidado incondicional y por estar siempre a mi lado, no solo en mi infancia, sino a lo largo de todo mi crecimiento. Su apoyo inquebrantable ha sido un pilar fundamental en mi vida. A mi abuelita Josefina, por su cariño y sabiduría, y a mi familia en general, por ser mi soporte constante, por creer en mí cuando más lo necesitaba y por darme todo sin esperar nada a cambio.

Y a mi compañera Ana Emilia, por su gran ayuda en la realización de esta tesis. Su dedicación al estudio, su perseverancia y su apoyo cuando todo se volvió difícil o confuso, fueron fundamentales para lograr este objetivo.

*William Cruz*

# AGRADECIMIENTO

Agradezco a mi profesor Óscar Camacho por brindarme la oportunidad de realizar esta tesis bajo su tutoría y por confiar en mi trabajo desde el inicio. Su orientación, exigencia académica y constante apoyo fueron clave para el desarrollo de este proyecto.

A mi familia, por su amor incondicional, por estar presente en cada etapa y por ser mi mayor fuente de fortaleza a lo largo de mi vida. Su apoyo constante, sus palabras de aliento y su ejemplo diario han sido clave para alcanzar este objetivo.

Y a mi compañero, William, por su colaboración, perseverancia, disciplina y determinación para avanzar, incluso cuando el camino se volvió desafiante.

*Ana Emilia Ludeña*

# CHAPTER 1

## INTRODUCTION

Aerospace and mechatronic applications have evolved significantly, becoming a central focus in automation and control engineering. Unmanned Aerial Vehicles (UAVs) and drones have emerged as essential tools across various sectors, from security and surveillance to precision agriculture (Fellag and Belhocine, 2024). Consequently, designing effective control strategies for these dynamic systems remains a key research area.

The Quanser Aero 2 platform, developed for educational and research purposes (Quanser, ), offers a compact aerospace laboratory equipped with two configurable rotors (1-DOF or 2-DOF), capable of simulating the dynamics of a half-quadrotor system (Quanser Inc., 2022). This platform serves as an ideal testbed for validating control algorithms for UAVs and autonomous aerial vehicles.

Controlling aerial systems presents challenges due to delays, nonlinearities, and external disturbances (Beard and McLain, 2012). Although the Proportional-Integral-Derivative (PID) controller has been widely adopted for its simplicity (Åström and Hägglund, 1995), its fixed structure limits its adaptability in complex dynamic environments (Ogata, 2010). Recent research has led to the development of enhanced PID variants, including the two-degree-of-freedom PID (2-DOF) that decouples reference tracking and disturbance rejection (Taguchi and Araki, 2000); the Fractional-Order PID (FOPID) that introduces non-integer operators for greater dynamic flexibility (Herrera et al., 2023); the Nonlinear PID (NPID) that adjusts gains based on error magnitude (Quiñónez et al., 2019, Proaño et al., 2025); and the Intelligent PID (iPI) based on model-free control principles (Fliess and Join, 2013).

In this study, a comparative experimental evaluation of different PID controller approaches is conducted for the 1-DOF Quanser Aero 2 system. The classical PID controller serves as the baseline, and several improved variants are compared, including 2-DOF PID, fractional-order PID, nonlinear PID (all model-based), as well as the model-free iPI approach. The results demonstrate that these enhanced controllers can improve system performance under varying reference inputs and external disturbances. The 1-DOF configuration is specifically selected as it simulates real-world scenarios such as pitch control during UAV takeoff and landing, where angular stability is crucial (Pounds et al., 2006, Tayebi and McGilvray, 2006). All controller parameters are tuned using genetic algorithms to ensure a fair comparison. The performance indicators employed in this study are the Integral of Absolute Error (IAE), Integral of Squared Control Output (ISCO), maximum overshoot, and settling time.

The document is organized as follows: Section 2 presents the mathematical model of the Quanser Aero 2 platform. Section 3 describes the control techniques employed. Section 4 discusses the experimental results and the performance metrics used to evaluate each control strategy. Finally, Section 5 presents the conclusions and future research directions.

# CHAPTER 2

# QUANSER AERO 2 FUNDAMENTALS

The Quanser AERO 2 is a tabletop device, Fig. 2.1, designed for education and research in flight dynamics and control. It simulates a helicopter system with 2 degrees of freedom, where pitch and yaw are adjusted using propellers. This platform is ideal for practical learning in control systems, dynamics, and aerospace engineering. It facilitates real-time experiments and controller design when integrated with MATLAB/Simulink.

Figure 2.1: Quanser Aero 2 plant.

### 2.0.1 Mathematical Modeling

The Quanser Aero 2 system is modeled by analyzing the rotational dynamics around the pitch axis. Key variables and parameters are listed in Table 2.1.

Table 2.1: System Variables, Parameters, and Acting Torques

| Symbol | Description | Units |
|---|---|---|
| $\theta(t)$ | Pitch angle | rad |
| $\dot{\theta}(t)$ | Pitch angular velocity | rad/s |
| $\ddot{\theta}(t)$ | Pitch angular acceleration | rad/s$^2$ |
| $J_p$ | Moment of inertia | kg·m$^2$ |
| $D_p$ | Viscous damping coefficient | N·m/(rad/s) |
| $K_{sp}$ | Pitch stiffness | N·m/rad |
| $T_p(t)$ | External torque (rotor) | N·m |
| $d_t$ | Thrust offset from axis | m |
| $K_{pp}$ | Thrust gain | N/m |
| $M_b$ | Aero body mass | kg |
| $D_m$ | COM distance from axis | m |
| $\tau_{\text{inertia}} = J_p \cdot \ddot{\theta}(t)$ | Inertial torque | N·m |
| $\tau_{\text{damping}} = D_p \cdot \dot{\theta}(t)$ | Damping torque | N·m |
| $\tau_{\text{restoring}} = K_{sp} \cdot \theta(t)$ | Restoring (spring) torque | N·m |
| $\tau_{\text{rotor}} = T_p(t)$ | Rotor torque (external input) | N·m |

**Dynamic Equation Derivation**

Applying Newton's second law for rotation:

$$\sum \tau = J_p \cdot \ddot{\theta}(t) \tag{2.1}$$

Thus, the motion equation becomes:

$$J_p \cdot \ddot{\theta}(t) + D_p \cdot \dot{\theta}(t) + K_{sp} \cdot \theta(t) = T_p(t) \tag{2.2}$$

**Rotor Torque Modeling**

The rotor torque is defined as:

$$T_p(t) = F_{\text{thrust}}(t) \cdot d_t = K_{pp} \cdot \omega_n(t) \cdot d_t \tag{2.3}$$

**Final Dynamic Model**

Substituting into the motion equation:

$$J_p \cdot \ddot{\theta}(t) + D_p \cdot \dot{\theta}(t) + K_{sp} \cdot \theta(t) = K_{pp} \cdot \omega_n(t) \cdot d_t \tag{2.4}$$

**Transfer Function**

Using the Laplace transform with zero initial conditions:

$$\frac{\Theta(s)}{\omega_n(s)} = \frac{K_{pp} \cdot d_t}{J_p s^2 + D_p s + K_{sp}} \tag{2.5}$$

**Normalized Form**

Dividing by $J_p$ yields the normalized transfer function:

$$\frac{\Theta(s)}{\omega_n(s)} = \frac{K_{pp} \cdot d_t / J_p}{s^2 + \frac{D_p}{J_p} s + \frac{K_{sp}}{J_p}} \tag{2.6}$$

This model accurately captures the pitch-axis dynamics and serves as the foundation for controller design and simulation in Simulink.

The parameter values in Table 2.2 are specific to the pitch dynamics of the Quanser Aero 2 used in this study. While these values are kept constant throughout the simulations, they can be modified to reflect changes in environmental conditions or system calibration.

Table 2.2: Parameter Values of the System

| **Parameter** | **Description** | **Value** |
|---|---|---|
| $K_{sp}$ | Pitch stiffness | 0.0204 N·m/rad |
| $D_p$ | Viscous damping coefficient | 0.00104 N·m/(rad/s) |
| $K_{pp}$ | Thrust force gain | $2.52 \times 10^{-4}$ N/m |
| $M_b$ | Mass of the Aero body | 1.07 kg |
| $d_t$ | Distance of thrust from the axis | 0.167 m |
| $J_p$ | Moment of inertia | 0.0232 kg·m$^2$ |

The following parameters and values were provided by the official documentation of the Quanser Aero 2 system, (Quanser Inc., 2022).

# CHAPTER 3

# CONTROL TECHNIQUES FUNDAMENTALS

This section outlines the control strategies utilized in this study. The analysis covers five controllers: the traditional PID, 2-DOF PID, FOPID, and NPID, all of which are model-based, alongside the iPI, a model-free or data-driven controller that relies solely on input-output data. This arrangement facilitates a comparison between the effectiveness of model-specific and model-independent approaches in dynamic environments. The controllers are engineered to modify the rotor speeds in order to control the pitch angle $\theta$ of the Quanser Aero 2.

### 3.0.1 Proportional-Integral-Derivative (PID)

The PID controller is widely adopted in industrial systems for its simplicity and effectiveness in regulation tasks (Åström and Hägglund, 1995). It combines proportional, integral, and derivative actions to reduce error, eliminate steady-state offset, and improve transient response, respectively. Its control law is as follows:

$$u(t) = K_p e(t) + K_i \int e(t)\,dt + K_d \frac{de(t)}{dt} \tag{3.1}$$

where $K_p$, $K_i$, and $K_d$ are the proportional, integral, and derivative gains, $e(t) = r(t) - y(t)$ is the tracking error , $r(t)$ is the reference and $y(t)$ the output of the process (Camacho et al., 2020).

### 3.0.2 Two-Degree-of-Freedom PID (2-DOF PID)

The 2-DOF PID controller extends the classical PID by decoupling reference tracking from disturbance rejection, offering greater tuning flexibility (Taguchi and Araki, 2000). It modifies the proportional and derivative actions using weighting factors $\beta$ and $\gamma$:

$$u(t) = K_p[\beta \cdot r(t) - y(t)] + K_i \int [r(t) - y(t)]\, dt + K_d[\gamma \cdot \dot{r}(t) - \dot{y}(t)] \tag{3.2}$$

where $\beta, \gamma \in [0, 1]$. This structure helps reduce overshoot and derivative kick during setpoint changes, while preserving robustness against disturbances. The controller is tested on the Aero 2 platform to assess its benefits over the classical PID.

### 3.0.3 Fractional-Order PID (FOPID)

The FOPID controller is a generalization of the classical PID controller (Vega et al., 2024). Its structure can be expressed as:

$$G_{FOPID}(s) = K_p \left(1 + \frac{1}{T_i s^{\lambda}} + T_d s^{\mu}\right). \tag{3.3}$$

This fractional configuration incorporates two tuning factors, $\lambda$ and $\mu$ ($\lambda, \mu \in \mathbb{R}^+$), thus increasing the number of tunable parameters from three to five. This expands upon the traditional PID controller, with the conventional PID configuration being restored by setting $\lambda$ and $\mu$ to 1.

FOPID controllers offer improved robustness, stability margins, and better performance in reference tracking and disturbance rejection compared to classical PID controllers (Vega et al., 2024), making them well suited for systems with complex or uncertain dynamics.

This study implemented the FOPID controller using the Toolbox **FOMCON**, a MATLAB and Simulink-based toolbox for fractional-order control (Tepljakov et al., 2019).

### 3.0.4 Nonlinear PID (NPID)

In traditional PID controllers, the control actions (proportional, integral, and derivative) are generated based on a constant error signal, which is used to compute the controller gains. However, in many practical applications, the linear nature of a standard PID controller is insufficient to handle nonlinearities within the system. To address this, Nonlinear PID (NPID) controllers were developed, which introduce a nonlinear gain in cascade with a traditional PID controller (Proaño et al., 2025).

The general form of a nonlinear PID controller can be described as:

$$u(t) = K_p(\cdot) \cdot e(t) + K_i(\cdot) \int_0^t e(t)dt + K_d(\cdot)\frac{d}{dt}e(t) \tag{3.4}$$

Where $K_p(\cdot)$, $K_i(\cdot)$, and $K_d(\cdot)$ are time-varying gains, and $e(t)$ is the error signal. These time-varying gains are modeled using nonlinear functions that depend on the system error. The nonlinear function allows for different behavior depending on the size of the error.

Various nonlinear functions can be used for this gain, including smooth sigmoidal functions. The sigmoidal function used in this case is expressed as:

$$k_e = k_0 + k_1 \left( \frac{2}{1 + e^{-k_2 e}} - 1 \right) \tag{3.5}$$

The parameters $k_0$, $k_1$, and $k_2$ define the characteristics of the sigmoidal function. Specifically, $k_0$ sets the central value of the nonlinear gain, $k_1$ determines the range of variation, and $k_2$ controls the rate of change. The gain $k(e)$ is bounded between $k_{\text{min}} = k_0 - k_1$ and $k_{\text{max}} = k_0 + k_1$, with typical conditions ensuring $k_1 \leq k_0$ to maintain positive gains. This configuration allows precise adjustment of the controller's sensitivity depending on the magnitude of the system error (Quiñónez et al., 2019).

### 3.0.5 Intelligent Proportional-Integral (iPI) Controller

Model-free control aims to bypass the need for explicit modeling of system dynamics. Instead, the behavior of the system is approximated by a simple ultra-local model:

$$y^{(v)}(t) = F(t) + \alpha u(t) \tag{3.6}$$

where $y^{(v)}(t)$ denotes the $v$-th time derivative of the output $y(t)$, $u(t)$ is the control input, $\alpha$ is a tuning parameter, and $F(t)$ aggregates all unknown system dynamics and external disturbances.

This framework enables the design of robust controllers, such as the Intelligent Proportional-Integral (iPI) controller, without relying on detailed physical models, significantly simplifying implementation (Fliess and Join, 2013).

The Intelligent PI (iPI) controller is derived from the ultra-local model and eliminates the need for exact system identification. Its control law is given by:

$$u(t) = \frac{1}{\alpha}\left[-\hat{F}(t) + \dot{r}(t) + K_p e(t) + K_i \int_0^t e(t)dt\right] \tag{3.7}$$

The reference trajectory is represented by $r(t)$, while $\hat{F}(t)$ serves as an online approximation of $F(t)$, generally calculated through numerical differentiation.

The iPI controller exhibits strong robustness against modeling uncertainties and external perturbations, making it highly suitable for practical applications where accurate models are unavailable or expensive to derive.

# CHAPTER 4

# RESULTS AND DISCUSSION

### 4.0.1 Model Identification and Analysis

To implement the different PID controller alternatives, we characterize the plant. The system under study operates in a cascaded configuration, comprising a motor and a pitch mechanism, as illustrated in Figure 4.1. The primary objective was to begin with the classical PID controller by analyzing the system's response to a step input using MATLAB's Model Analyzer.

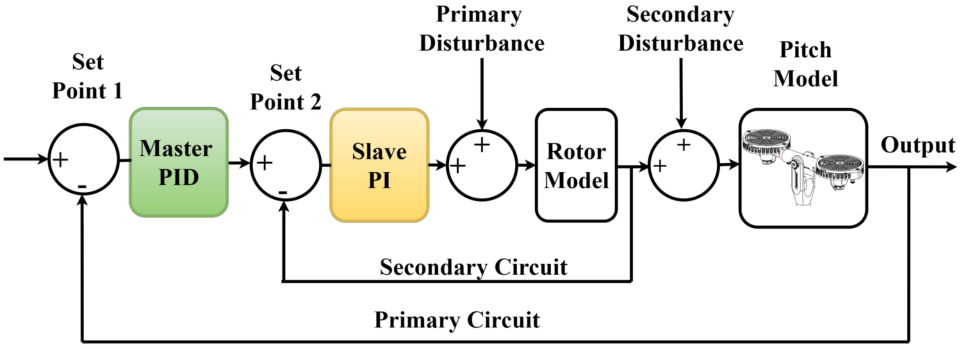


Figure 4.1: Block diagram of the cascade control system.

#### System Linearization and State-Space Representation

The plant was linearized at its initial operating point using MATLAB's Model Analyzer, resulting in the following continuous-time state-space representation:

$$A = \begin{bmatrix} -0.04485 & -0.8797 & 0 & 115.4 \\ 1 & 0 & 0 & 0 \\ 0 & -0.0182 & 0 & -1154 \\ 0 & 0 & 1 & -63.89 \end{bmatrix}, \quad B = \begin{bmatrix} 0 \\ 0 \\ 3 \\ 0 \end{bmatrix}$$

$$C = \begin{bmatrix} 0 & 0.00182 & 0 & 0 \end{bmatrix}, \quad D = \begin{bmatrix} 0 \end{bmatrix}$$

The state variables are defined as follows:

- $x_1$: Pitch angle (Model 1)
- $x_2$: Pitch rate (Model 2)
- $x_3$: Integrator state
- $x_4$: Rotor dynamics

The input $u_1$ corresponds to the control signal applied to the system, and the output $y_1$ represents the measured pitch angle.

**Transfer Function Derivation**

From the linearized state-space model, the transfer function from input $u_1$ to output $y_1$ was derived:

$$G(s) = \frac{2.1}{s^4 + 63.93s^3 + 1158s^2 + 108s + 1016} \tag{4.1}$$

This fourth-order transfer function indicates the presence of four energy storage elements within the system, corresponding to the four state variables identified earlier.

**Closed-Loop System and Stability Analysis**

To analyze the closed-loop behavior, a proportional controller with gain $k$ was considered. The closed-loop transfer function is given by:

$$G_{cl}(s) = \frac{k \cdot G(s)}{1 + k \cdot G(s)} \tag{4.2}$$

$$G_{cl}(s) = \frac{2.1k}{s^4 + 63.93s^3 + 1158s^2 + 108s + 1016 + 2.1k} \tag{4.3}$$

To study the stability of any control system, control theory says that we need only to look at the characteristic equation of the system:

$$s^4 + 63.93s^3 + 1158s^2 + 108s + (1016 + 2.1k) = 0 \tag{4.4}$$

Utilizing the substitution method (Smith, 2002) related to the Ziegler–Nichols closed loop marginal stability approach, the critical gain $K_{cu}$ and the critical period $P_u$ are determined by analyzing the closed-loop characteristic Eq. (4.4), by substituting $s = j\omega$, the result is as follows:

$$(j\omega)^4 + 63.93(j\omega)^3 + 1158(j\omega)^2 + 108(j\omega) + (1016 + 2.1 \cdot k) = 0 \tag{4.5}$$

Separating into real and imaginary parts:

- Real part:

$$\omega^4 - 1158\omega^2 + (1016 + 2.1 \cdot k) = 0 \tag{4.6}$$

- Imaginary part:

$$-63.93\omega^3 + 108\omega = 0 \tag{4.7}$$

$$\omega(-63.93\omega^2 + 108) = 0$$

- Solving:

$$\omega^2 = \frac{108}{63.93} \approx 1.689 \quad \Rightarrow \quad \omega \approx 1.3\,\text{rad/s}$$

With the natural frequency $\omega$ obtained, the critical period is computed as:

$$P_u = \frac{2\pi}{\omega} = \frac{2\pi}{1.3} \approx 4.83\,\text{s}$$

$$\boxed{P_u \approx 4.83 \text{ s}} \tag{4.8}$$

By substituting the value of $\omega$ into the equation for the real part, the critical gain can be determined as shown:

$$\boxed{k = K_{cu} < 441.2} \tag{4.9}$$

### 4.0.2 PID Controller Parameters Using the Ziegler–Nichols Method

The resulting values of $K_{cu}$ and $P_u$ are used to compute the PID gains, following the standard tuning rules summarized in Table 4.1, based on the Ziegler–Nichols formulas compiled by (Camacho et al., 2020). These values correspond to the initial tunings for the PID controller.

Table 4.1: Ziegler–Nichols PID tuning equations and calculated values (Camacho et al., 2020)

| **Parameter** | **Equation** | **Value** |
|---|---|---|
| Proportional gain | $K_p = \frac{K_{cu}}{1.7}$ | 262 |
| Integral gain | $K_i = \frac{K_p}{P_u/2}$ | 108 |
| Derivative gain | $K_d = K_p \cdot \frac{P_u}{8}$ | 158 |

### 4.0.3 Optimal tuning using Genetic Algorithms

The Genetic Algorithm (GA) is a model of biological evolution inspired by Charles Darwin's theory of natural selection. It was developed by John Holland as a method for solving complex optimization problems through adaptive processes (Lambora et al., 2019). In this work, the GA is applied to automatically tune the parameters of a PID controller ($Kp$, $Ki$, and $Kd$). The algorithm begins with a population of randomly generated candidate solutions, each representing a possible set of PID gains. These candidates are evaluated by simulating the control system and measuring their performance using two criteria: **IAE** (Integral of Absolute Error) and **ISCO** (Integral of Squared Control Output). These metrics reflect tracking accuracy and control effort, respectively (MathWorks, 2023).

The multi-objective function (FO) is defined as follows:

$$
\begin{aligned}
f_{\text{IAE}} &= \begin{cases} \text{IAE} + 100, & \text{if IAE} > 10^{-5} \\ \text{IAE}, & \text{otherwise} \end{cases} \\
f_{\text{ISCO}} &= \begin{cases} \text{ISCO} + 100, & \text{if ISCO} > 10^{-5} \\ \text{ISCO}, & \text{otherwise} \end{cases}
\end{aligned}
\tag{4.10}
$$

$$
\text{FO} = \int \text{IAE}\, dt + \int \text{ISCO}\, dt \tag{4.11}
$$

The best-performing solutions are selected and used to generate a new population through crossover and mutation. This evolutionary cycle continues until a stopping condition is met, such as reaching a predefined number of generations or achieving an acceptable performance level (Lambora et al., 2019).

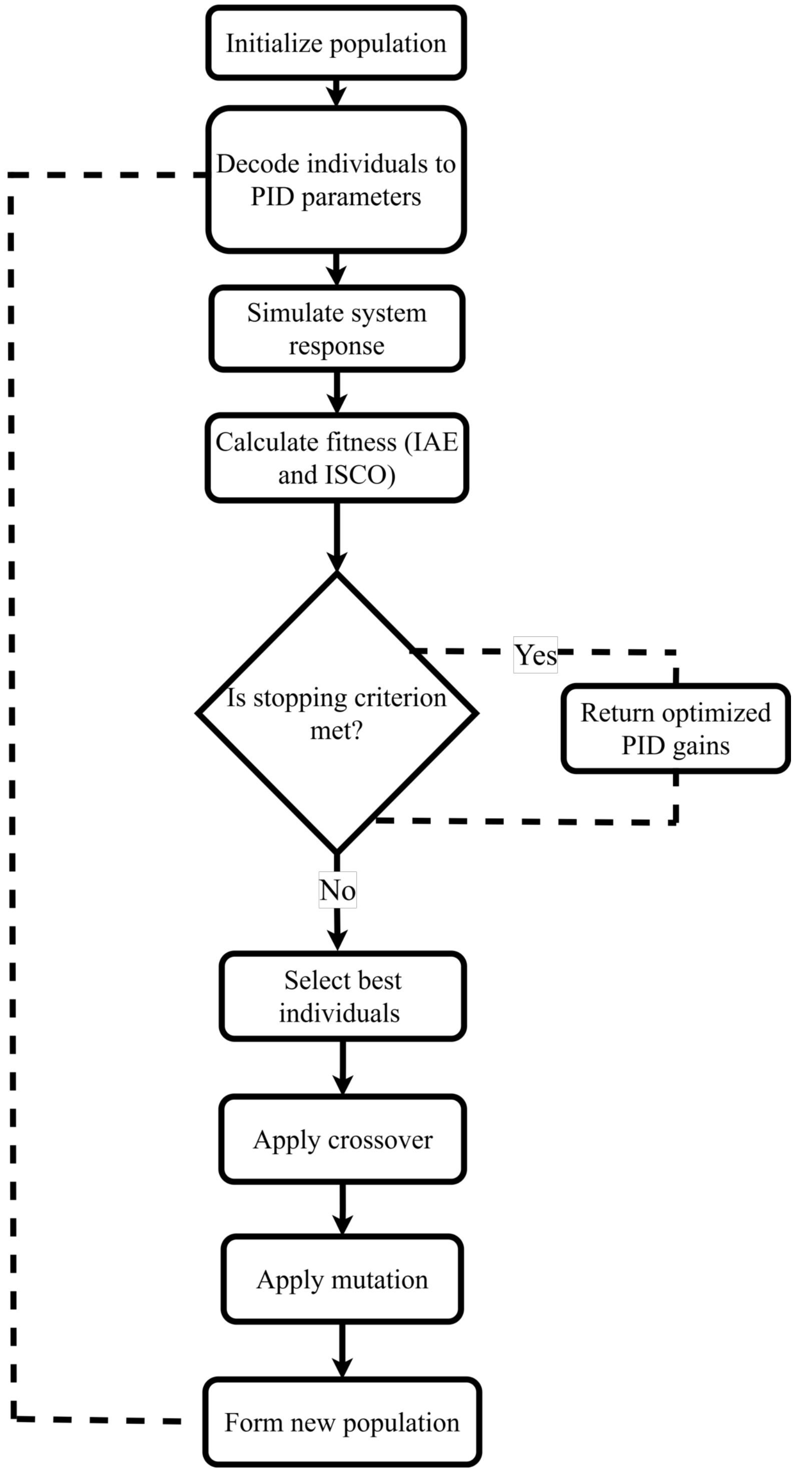


Figure 4.2: Flowchart of the Genetic Algorithm used for tuning all PID-based controllers.

This approach was employed to tune all PID-based controllers, achieving a balance between tracking accuracy and control effort. The optimized parameter values obtained through the Genetic Algorithm are presented in Table 4.2.

Table 4.2: Final tuning parameters used in the experimental implementation of each controller

| **Parameter** | **PID** | **2-DOF PID** | **FOPID** | **NPID** | **iPI** |
|---|---|---|---|---|---|
| $K_p$ | 235 | 440 | 120 | – | – |
| $K_i$ | 240 | 280 | 210 | 100 | – |
| $K_d$ | 490 | 500 | 400 | 300 | – |
| $b$ | – | 1 | – | 0 | – |
| $c$ | – | 0 | – | – | – |
| $\mu$ | – | – | 0.8 | – | – |
| $\lambda$ | – | – | 1.001 | – | – |
| $k_0$ | – | – | – | 0.7 | – |
| $k_1$ | – | – | – | $\pi/2$ | – |
| $k_2$ | – | – | – | -0.5 | – |
| $a$ | – | – | – | 1 | – |
| $K_{p1}$ | – | – | – | – | 0.1 |
| $K_{i1}$ | – | – | – | – | 70 |
| $K_{LP1}$ | – | – | – | – | 100 |
| $T_{LP1}$ | – | – | – | – | 0.4 |
| $T_{LP2}$ | – | – | – | – | 0.1 |
| $K_{LP2}$ | – | – | – | – | 200 |

### 4.0.4 Experimental Results

To evaluate the performance of each controller, two experimental scenarios were conducted on the Quanser Aero 2 platform in its 1-DOF configuration. The first assessed the tracking of a reference change, generated by a *Pulse Generator* block, while the second was introduced to an external disturbance at 50 seconds. All tests respected the platform's input voltage limits of $[-24, 24]$ V.

The control algorithms were deployed through the QUARC real-time control software in MATLAB/Simulink, with a sampling time of 0.01s. In addition, the system responses were analyzed using performance metrics such as IAE, ISCO, overshoot, and settling time.

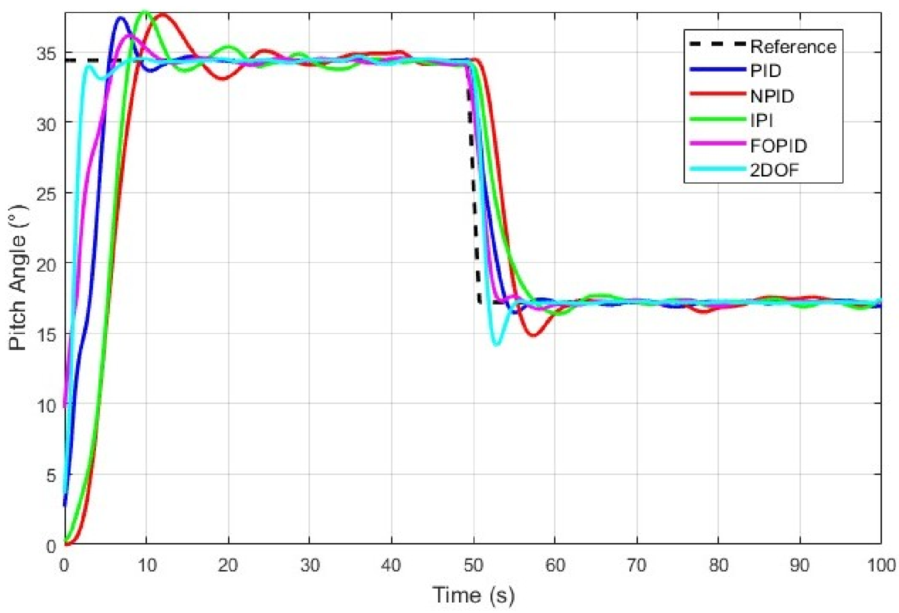


Figure 4.3: Pitch angle response of PID-based controllers to a reference change on the Quanser Aero 2 system.

Figure 4.3 shows the controllers' responses to a reference change. All schemes successfully reach the new setpoint, but exhibit different dynamic behaviors. Some controllers present noticeable overshoot and oscillations, while others provide smoother and more stable responses, highlighting a trade-off between speed and damping performance.

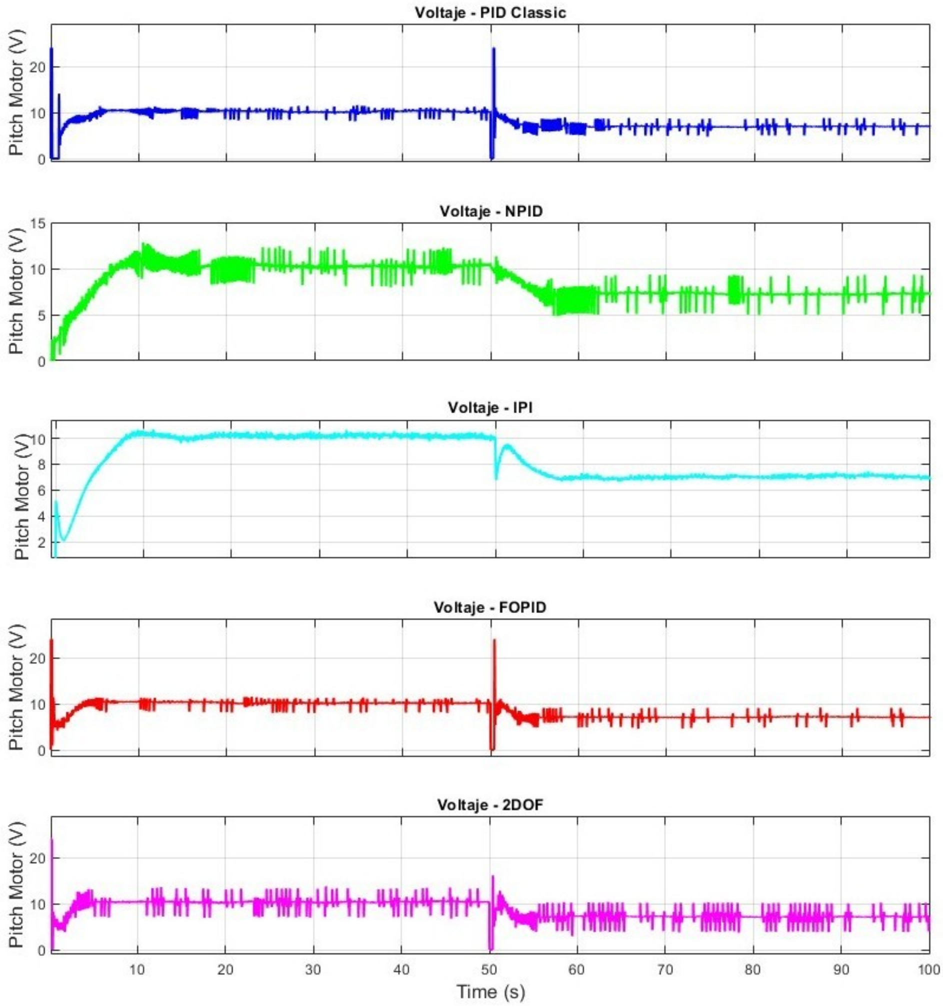


Figure 4.4: Voltage signals in response to a reference change for all tested controllers on the Quanser Aero 2.

Figure 4.4 and 4.7 demonstrates that each controller sustains a balanced voltage consumption in the pitch motor. Even with differences in control aggressiveness and response speed, all strategies avoid placing undue stress on the actuator, suggesting that the controllers effectively ensure both efficient and safe system performance.

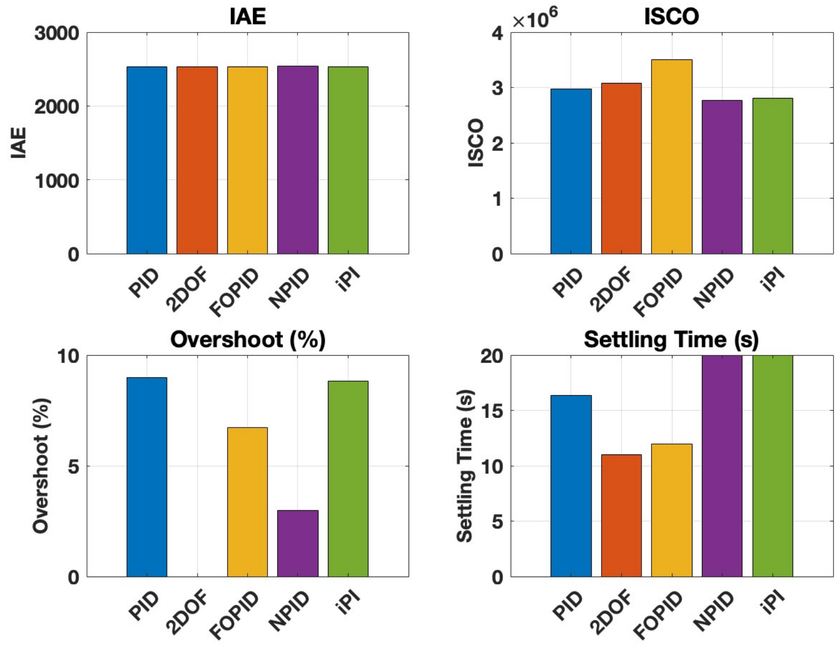


Figure 4.5: Performance metrics for reference tracking: IAE, ISCO, $M_p$, and $t_s$ for all controllers.

Figure 4.5 presents the performance metrics for reference tracking. All controllers achieved similar IAE values. In terms of control effort (ISCO), the FOPID required the most, while the NPID and iPI showed lower energy consumption. The PID and iPI exhibited the highest overshoot, around 9%, whereas the 2-DOF PID eliminated it. Regarding settling time, the 2-DOF PID and FOPID had the fastest responses (11–12 s), while the NPID and iPI were the slowest, reaching 20 s.

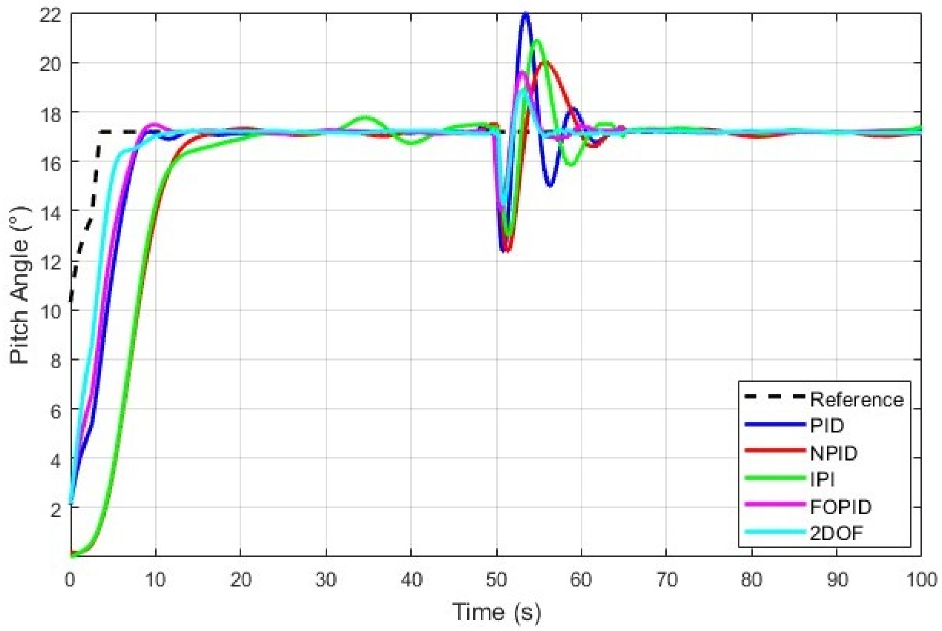


Figure 4.6: Pitch angle response of PID-based controllers to a disturbance input on the Quanser Aero 2 system.

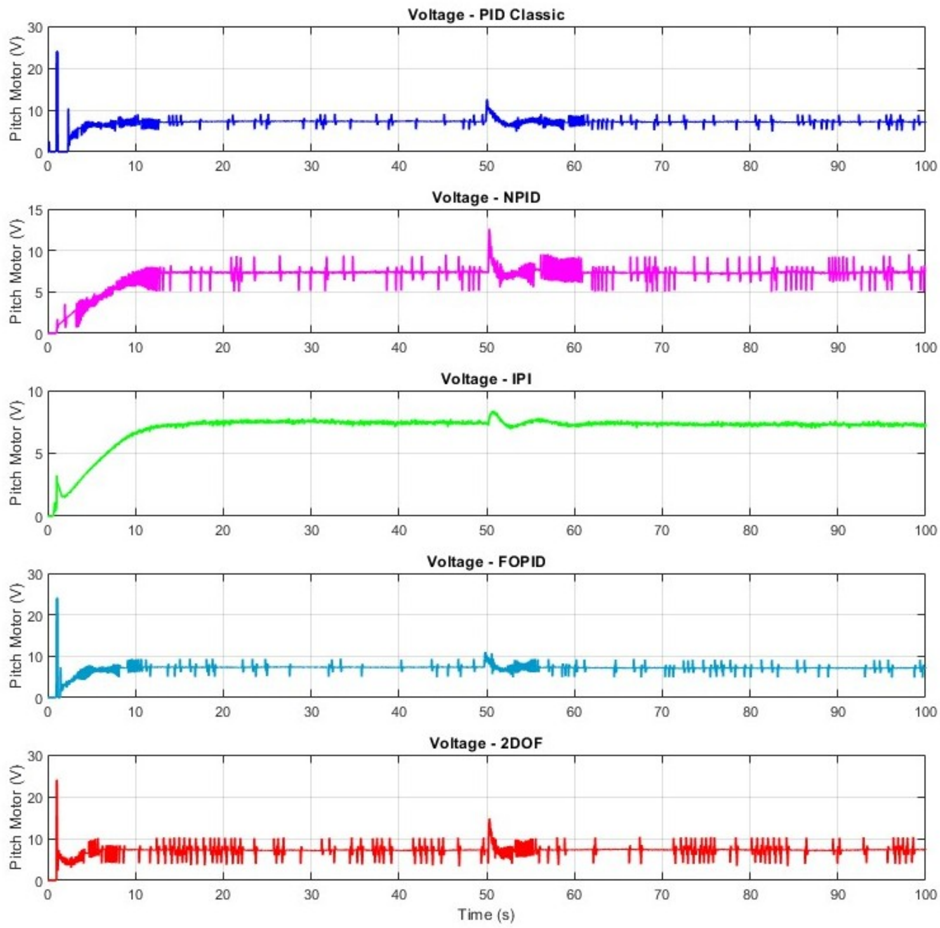


Figure 4.7: Voltage signals in response to an external disturbance for all tested controllers on the Quanser Aero 2.

Figure 4.6 presents the system response to an external disturbance applied at $t = 50\,\mathrm{s}$. Although the disturbance is identical for all controllers, their behavior varies significantly. The PID and NPID controllers display sharp peaks, whereas the IPI, FOPID, and 2-DOF PID controllers show better disturbance rejection, with smaller deviations and faster recovery, demonstrating greater robustness to external variations.

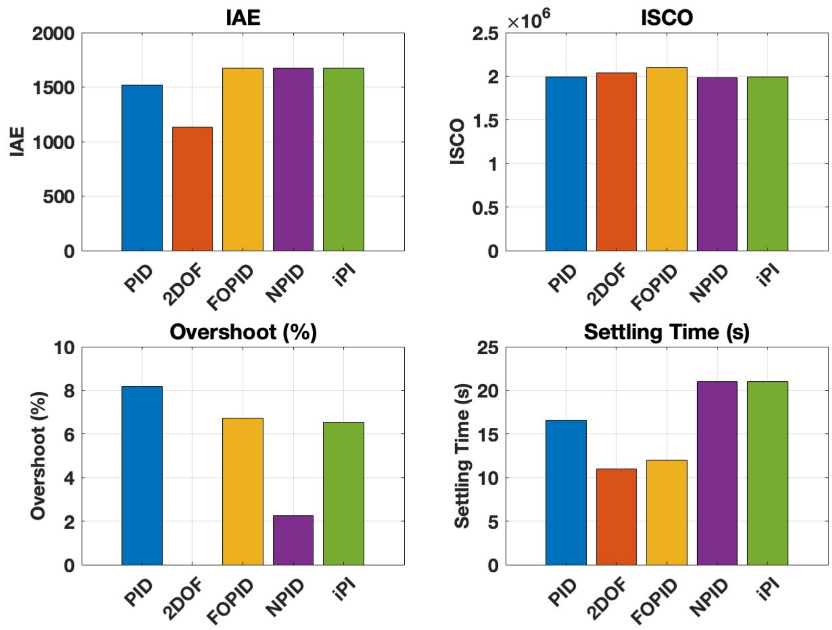


Figure 4.8: Performance metrics under disturbance rejection scenario: IAE, ISCO, $M_p$, and $t_s$ for each controller.

Figure 4.8 displays the performance metrics under a disturbance scenario. The 2-DOF PID achieved the lowest IAE, indicating superior disturbance rejection, while the PID and NPID also showed competitive accuracy. In terms of ISCO, all controllers maintained comparable control effort, with FOPID showing a slight increase. The 2-DOF PID again stood out by completely eliminating overshooting. Regarding settling time, the 2-DOF PID and FOPID demonstrated faster recovery, while the NPID and iPI took significantly longer to stabilize.

# CHAPTER 5

## CONCLUSIONS

This study evaluated various PID control strategies on the 1-DOF Quanser Aero 2 system. The classical PID controller served as a reference point for comparison with model-based 2-DOF PID, fractional-order PID, nonlinear PID, and the model-free iPI controller.

Utilizing genetic algorithms for parameter adjustment facilitated an equitable comparison of controllers with different architectures. Consequently, this method removed the bias of manual tuning and ensured uniformity in the evaluation criteria across all tested configurations.

The 2-DOF PID controller demonstrates superior performance, achieving a balance between reference tracking and effective disturbance rejection without compromising system stability or overloading the actuator.

The iPI controller exhibits a balanced performance in tracking and rejecting disturbances, showing only slight high-frequency oscillations in the controller outputs, which in turn contributes to the extended lifespan of the actuator component.

Future research should consider employing these controllers in Aero 2's full 2-DOF configuration to allow for evaluation within a more complex coupled dynamics.

# BIBLIOGRAPHY

Beard, R. W. and McLain, T. W. (2012). *Small Unmanned Aircraft: Theory and Practice*. Princeton University Press.

Camacho, O., Rosales, A., and Rivas, F. (2020). *Control de Procesos*. Escuela Politécnica Nacional.

Fellag, R. and Belhocine, M. (2024). Comparative analysis of pid, fuzzy pid, and anfis controllers for 2-dof helicopter trajectory tracking: simulation and hardware implementation. *Archive of Mechanical Engineering*, 71(3):323–349.

Fliess, M. and Join, C. (2013). Model-free control: Introduction and applications. `https://arxiv.org/pdf/1304.5640.pdf`.

Herrera, M., Teodoro, A. D., Villarroel, E., Benítez, D., and Camacho, O. (2023). Fractional-order pid controller: A performance evaluation for time delay systems. *2023 IEEE Chilean Conference on Electrical, Electronics Engineering, Information and Communication Technologies (CHILECON)*.

Lambora, A., Gupta, K., and Chopra, K. (2019). Genetic algorithm-a literature review. In *2019 international conference on machine learning, big data, cloud and parallel computing (COMITCon)*, pages 380–384. IEEE.

MathWorks (2023). How the genetic algorithm works. Accessed: 2025-05-04.

Ogata, K. (2010). *Modern Control Engineering*. Prentice Hall, 5th edition.

Pounds, P., Mahony, R., Corke, P., and Gresham, J. (2006). Towards dynamically-favourable quad-rotor aerial robots. In *Australasian Conference on Robotics and Automation*.

Proaño, P., Pozo, M., Gallardo, C., and Camacho, O. (2025). Non-linear pid control of ac current and dc voltage for a photovoltaic system operating on a microgrid. *Results in Control and Optimization*, 18:100514.

Quanser. Quanser aero. `https://www.quanser.com/products/quanser-aero/`. Accessed: 2024-04-16.

Quanser Inc. (2022). Quanser aero 2 – user manual.

Quiñónez, K., Camacho, O., and Chávez, D. (2019). Application of nonlinear pid controllers to bioreactor processes. In *2019 IEEE 4th Colombian Conference on Automatic Control (CCAC)*, pages 1–6.

Smith, C. A. (2002). *Automated continuous process control*. John Wiley & Sons.

Taguchi, H. and Araki, M. (2000). Two-degree-of-freedom pid controllers — their functions and optimal tuning. In *IFAC Workshop on Digital Control: Past, Present and Future of PID Control*, Terrassa, Spain.

Tayebi, A. and McGilvray, S. (2006). Attitude stabilization of a vtol quadrotor aircraft. *IEEE Transactions on Control Systems Technology*, 14(3):562–571.

Tepljakov, A., Petlenkov, E., Belikov, J., and Petráš, I. (2019). Fomcon toolbox for modeling, design and implementation of fractional-order control systems. *Applications in control*, 6:211–236.

Vega, S., Vasquez, M., Herrera, M., Puyol, D., Benítez, D., and Camacho, O. (2024). Comparative analysis and evaluation of fractional order controllers for systems with variable delay. In *2024 IEEE International Conference on Automation/XXVI Congress of the Chilean Association of Automatic Control (ICA-ACCA)*, pages 1–6. IEEE.

Åström, K. J. and Hägglund, T. (1995). *PID Controllers: Theory, Design, and Tuning*. Instrument Society of America, 2nd edition.